SCF^{Fbxl3} Ubiquitin Ligase Targets Cryptochromes at Their Cofactor Pocket

Weiman Xing[1,2], Luca Busino[3], Thomas R. Hinds[1], Samuel T. Marionni[4], Nabiha H. Saifee[1], Matthew F. Bush[4], Michele Pagano[3], Ning Zheng[1,2]

[1]Department of Pharmacology and [2]Howard Hughes Medical Institute, Box 357280, University of Washington, Seattle, Washington 98195, USA.
[3]Department of Pathology and Howard Hughes Medical Institute, NYU Cancer Institute, New York University School of Medicine, 550 First Avenue, MSB 599, New York, New York 10016, USA.
[4]Department of Chemistry, Box 351700, University of Washington, Seattle, Washington 98195, USA.

SUPPLEMENTARY INFORMATION

Contents

Supplementary Figure 1. Cryptochrome domain structure and sequence alignment.
Supplementary Figure 2. Native mass spectrometry analysis of mCRY2 (1-544).
Supplementary Figure 3. Superposition analysis of mCRY2-PHR and Dm (6-4)-photolyase.
Supplementary Figure 4. The ordered mCRY2-CCS region in the mCRY2-Fbxl3-Skp1 complex.
Supplementary Figure 5. Native mass spectrometry analysis of the mCRY2-Fblx3-Skp1 complex.
Supplementary Figure 6. Sequence alignment and structural elements of vertebrate Fbxl3.
Supplementary Figure 7. Interface between mCRY2 and Fbxl3-mCRY2.
Supplementary Figure 8. Sequence alignment of select regions of vertebrate cryptochromes.
Supplementary Figure 9. Interface between mCRY2 and Fbxl3-LRR-C.
Supplementary Figure 10. Period2 competes with Fbxl3 for binding CRYs.
Supplementary Figure 11. Phosphorylation sites mapped onto the mCRY2 structure.
Supplementary Figure 12. Comparison of LRR-containing F-box proteins with known structures

Supplementary Methods

Supplementary Table 1. Crystallographic data collection and refinement statistics.
Supplementary Table 2. Comparisons of mCRY2-PHR and select cryptochromes and (6-4)-photolyases of known structures.
Supplementary Discussion

Binding of reduced FAD to mCRY2-PHR
The role of two cysteines and a nearby salt bridge at the mCRY2-Fblx3 interface
Intracellular concentration of free FAD

Supplementary Figure 1. Cryptochrome domain structure and sequence alignment. a, Domain structures of *Arabidopsis thaliana* CRY1 (*At*CRY1), *Drosophila melanoganster* CRY (*Dm*CRY), and *Mus musculus* CRY1/2 (*Mm*CRY1/2). *Drosophila melanoganster* Dm(6-4)-photolyase is shown for comparison. **b**. Sequence alignment of the CCEs of vertebrate cryptochromes from *Mus musculus* (Mm), *Homo sapiens* (Hs), *Xenopus laevis* (Xl), *Gallus gallus* (Gg), and *Danio rerio* (Dr). Strictly conserved residues are colored in red. The N-terminal PHR sequences are omitted. Green cylinders, solid lines, and dash lines represent α-helical, loop, and disordered regions observed in the mCRY2-Fbxl3-Skp1 structure.

a.

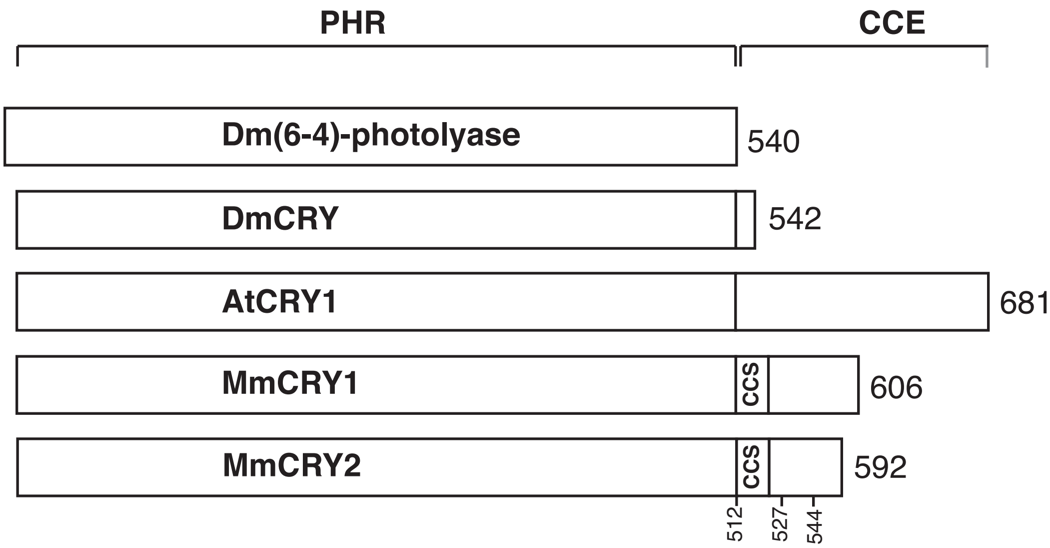

b.

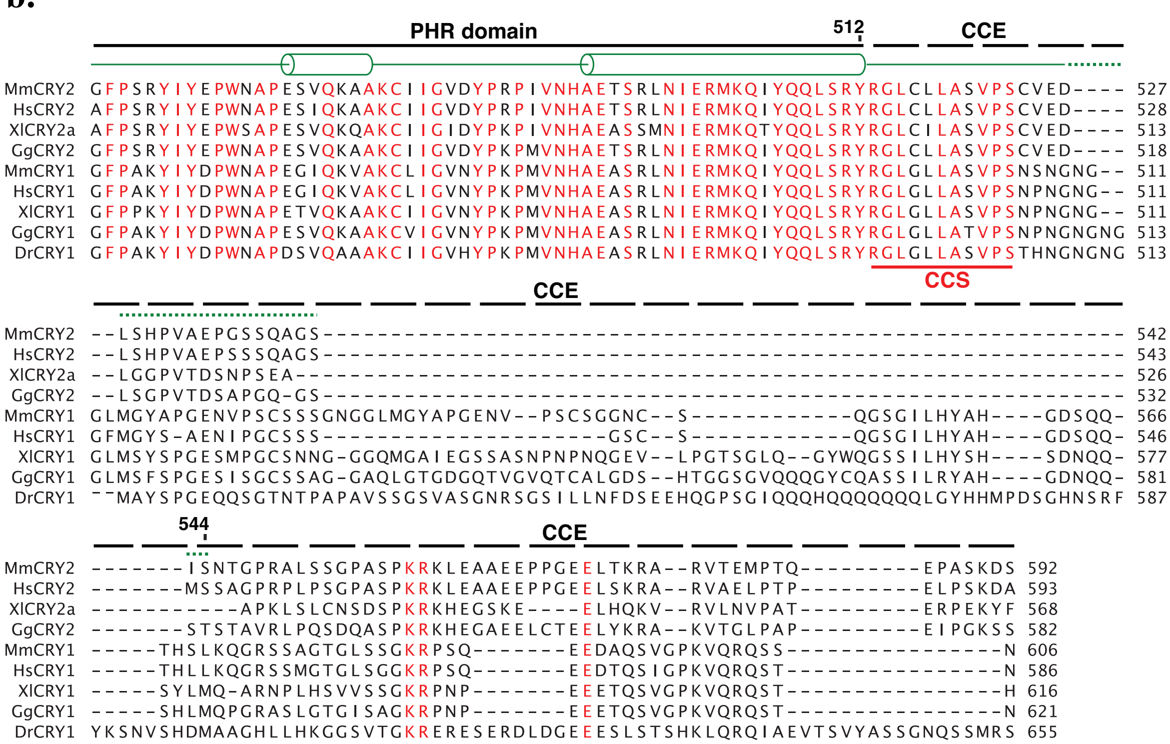

Supplementary Figure 2. Native mass spectrometry analysis of mCRY2 (1-544). Native mass spectra of mouse CRY2 (mCRY2) prepared as amino acids 1–544 (blue) and 1–512 (green) are shown in (a). The region containing the +15 charged protein ions is expanded in (b). Solid vertical lines show the expected *m*/*z* values for $(M_C+15H)^{+15}$ ions, where M_C corresponds the masses of various polypeptide chains terminated at different C-terminal positions, as indicated. The spectrum for mCRY2 (1-544) indicates that this sample has undergone significant degradation, and that the C-terminal residues of the resulting proteins were predominantly C516, L517, L518, A519, or S520. Interestingly, a second series of peaks were also observed that had a mass ~64 Da greater than those of the assigned peaks and are marked by vertical dotted lines. The origin of that mass difference has not been determined. The spectrum for mCRY2(1-512) is consistent with the expected chain length. The additional structure in that peak is attributable to ions containing different numbers of sodium ions instead of protons ($Na^+ - H^+ = 22$ Da).

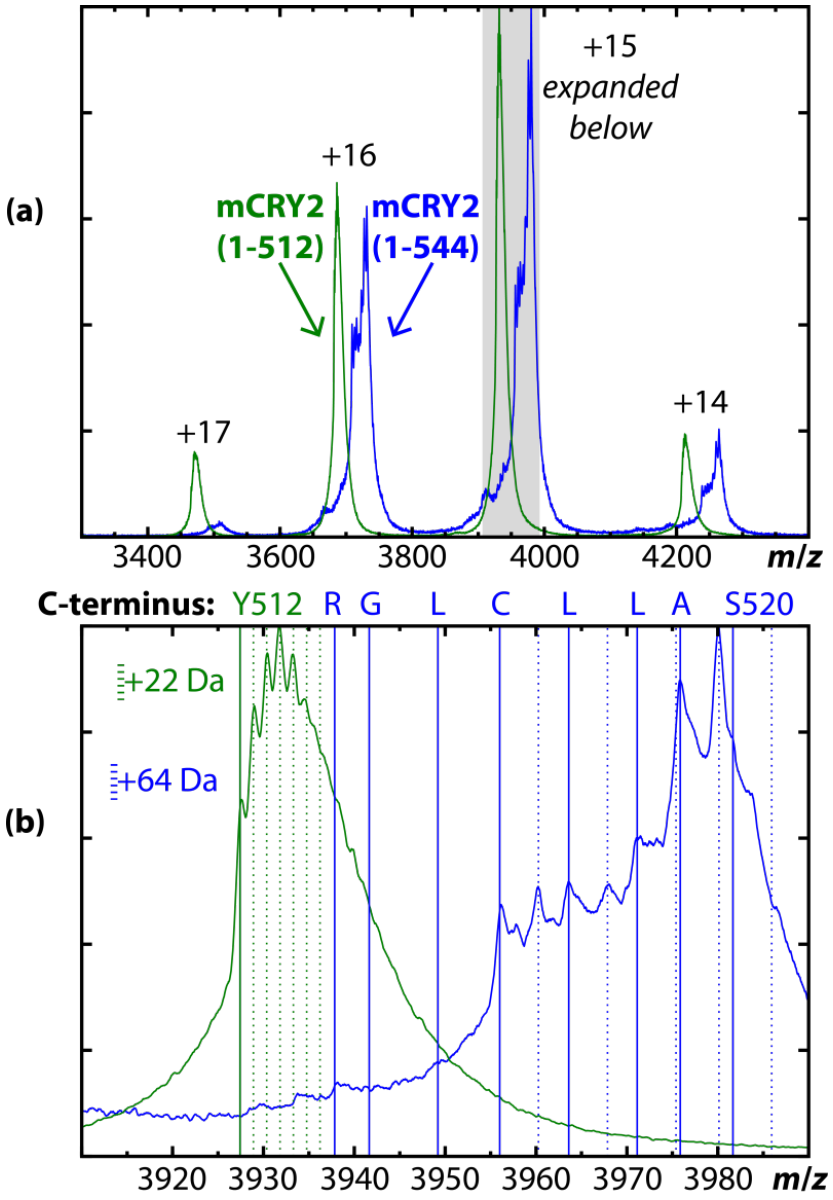

Supplementary Figure 3. Superposition analysis of mCRY2-PHR and Dm (6-4)-photolyase. Superimposed structures of mCRY2-PHR (slate blue) and *Drosophila melanoganster* (6-4)-photolyase (gray). The FAD cofactor of *Drosophila melanoganster* (6-4)-photolyase is shown in sticks.

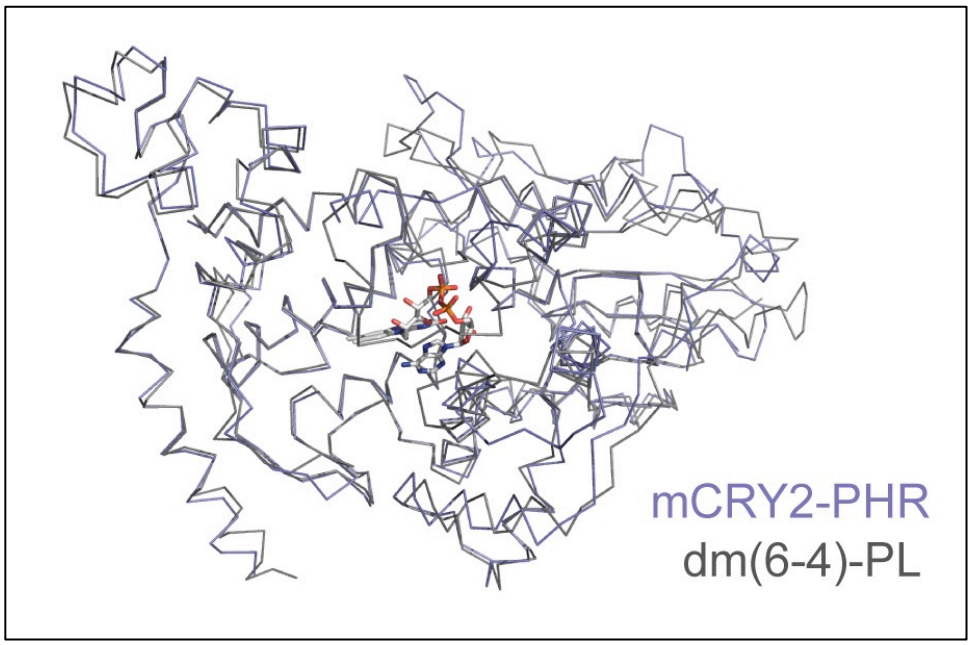

Supplementary Figure 4. The ordered mCRY2-CCS region in the mCRY2-Fbxl3-Skp1 complex. A close-up view of the CCS region of mCRY2 with unbiased omit map electron density contoured at 1 σ shown in mesh and amino acid side chains shown in sticks. The surrounding structural elements of Fbxl3 and mCRY2 are shown in magenta and slate blue ribbon diagrams, respectively. Both the CCS region and the C-terminal helix of mCRY2 are colored in cyan. Ala519 of mCRY2-CCS was not labeled due to space limitation. Although proteolytically stable, the C-terminal residues of mCRY2 beyond the CCS region showed no electron density in the crystal and were likely disordered.

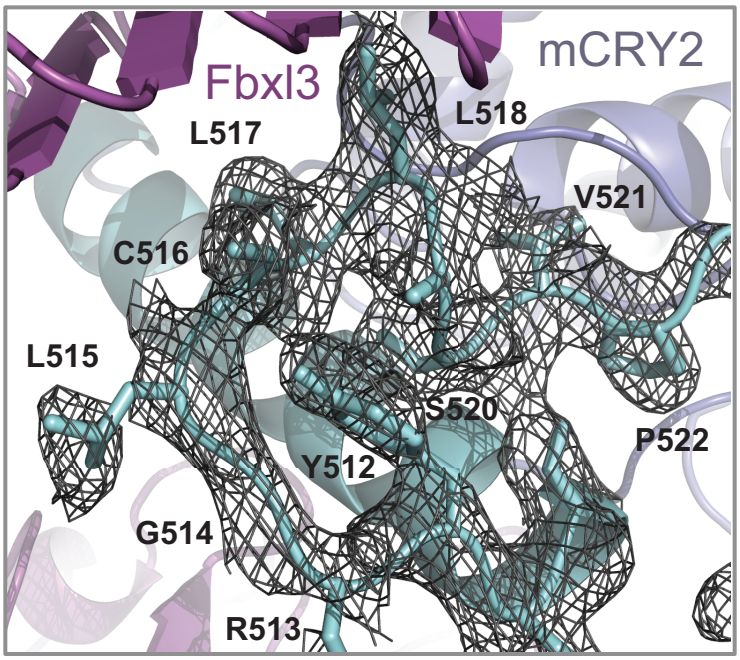

Supplementary Figure 5. Native mass spectrometry analysis of the mCRY2-Fblx3-Skp1 complex. The native mass spectrum of the mCRY2-Fbxl3-Skp1 complex is shown in (a), with the identities, masses for the expected sequences ($m_{sequence}$), and experimental masses ($m_{experimental}$). The +22 charge state of the mCRY2-Fbxl3-Skp1 complex (grey region in (a)) was isolated using a quadrupole mass filter, and activated using collision-induced dissociation (CID). CID results in the formation of Skp1 and mCRY2-Fbxl3 product ions, show in (b) and (c), respectively. Note that the spectra shown are from separate experiments; conditions were adjusted to improve spectral quality for the product ion of interest. The spectrum of the Skp1 product ion shows that $m_{experimental}$ is less than the expected mass for the full sequence of Skp1 (amino acids 1-149, 16 834 Da), suggesting the removal of the C-terminal lysine (amino acids 1-148, 16 706 Da). The expected *m*/*z* values for these two forms of Skp1 are marked on the expansion of the experimental data for the $(Skp1+10H)^{10+}$ ion. $m_{experimental}$ determined for the mCRY2-Fbxl3 product ion is consistent with the expected sequences without any phosphate group (+80 Da). Using this revised sequence for Skp1, $m_{experimental}$ for the mCRY2-Fbxl3-Skp1 complex is consistent with the revised $m_{sequence}$ and the absence of posttranslational modifications. A minor truncated form of the complex was also observed and is marked with (*). The location of the truncation has not been identified.

	Symbol	$m_{sequence}$	$m_{experimental}$
mCRY2-Fbxl3-Skp1		127 366 Da	127 340 ± 12 Da
mCRY2-Fbxl3-Skp1 (truncated)	*	N/A	124 291±1 Da
Skp1		16 706 Da	16 711 ± 1 Da
mCRY2-Fbxl3		110 678 Da	110 614 ± 7 Da

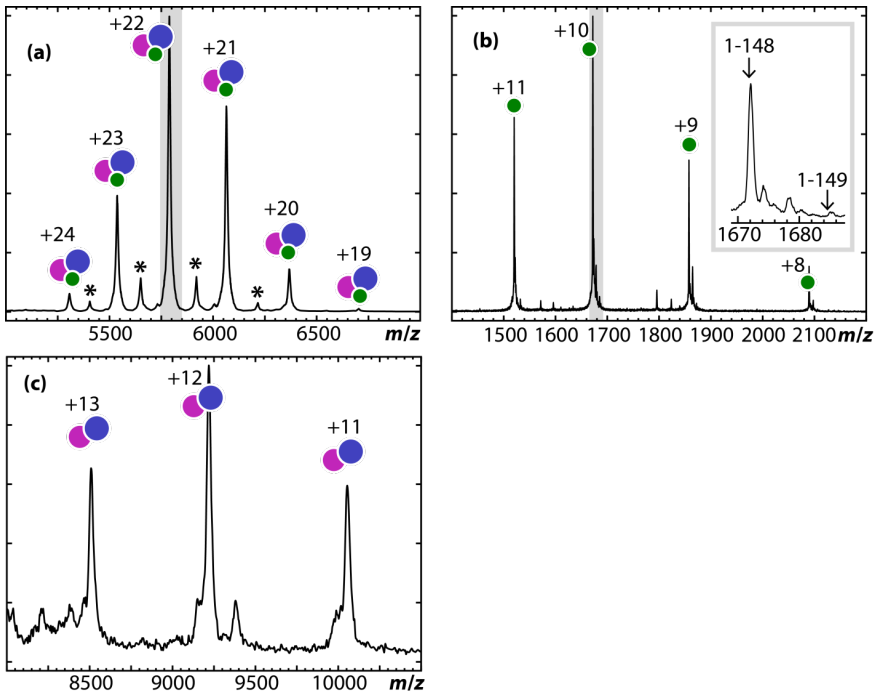

Supplementary Figure 6. Sequence alignment and structural elements of vertebrate Fbxl3. Alignment and secondary structure assignments of Fbxl3 orthologs from *Homo sapiens* (Hs), *Mus musculus* (Mm), *Xenopus tropicalis* (Xt), *Gallus gallus* (Gg), and *Danio rerio* (Dr). Strictly conserved residues are colored in black. Blue dots indicate mCRY2-interacting residues. Green squares indicate residues mutated in *overtime* and *after hours* alleles. Dash line represents the region of the protein disordered in the crystal.

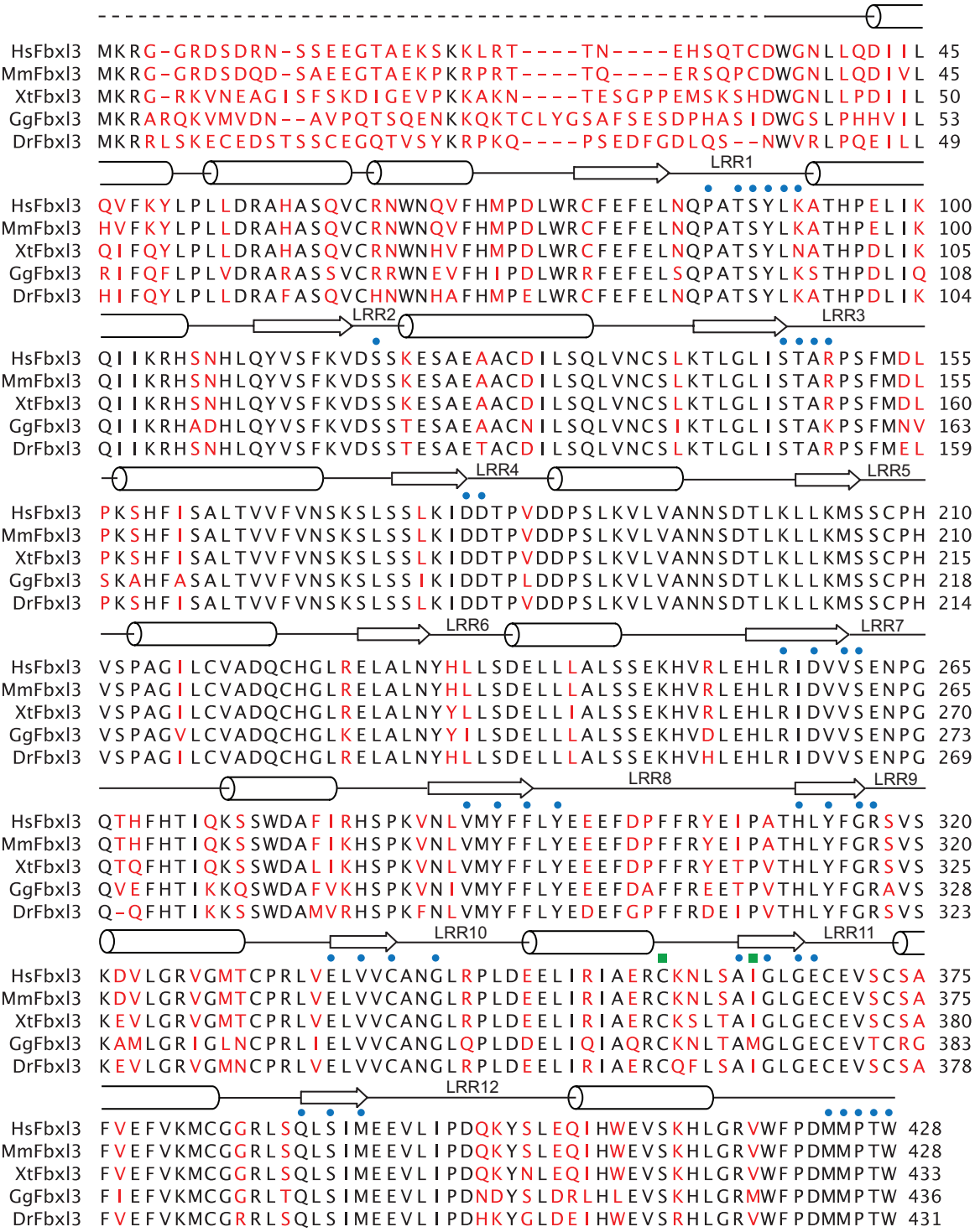

Supplementary Figure 7. Interface between mCRY2 and Fbxl3-mCRY2. a. The structural role of Pro422 in the C-terminal tail of Fbxl3. A close-up view of the C-terminal tail of Fbxl3, which takes a sharp turn at Pro422 before inserting into the FAD-binding pocket of mCRY2. Fbxl3 is shown in ribbon diagrams (magenta) and mCRY2 in surface representation (slate blue). The side chain of Fbxl3 Pro422 is shown in sticks (yellow). **b**. A close-up view of the mCRY2-Fbxl3 interface at the apical ridge of LRR-N with select interacting residues shown in sticks. Yellow dash lines represent salt bridges and hydrogen bonds. Fbxl3 LRRs are labeled by numbers.

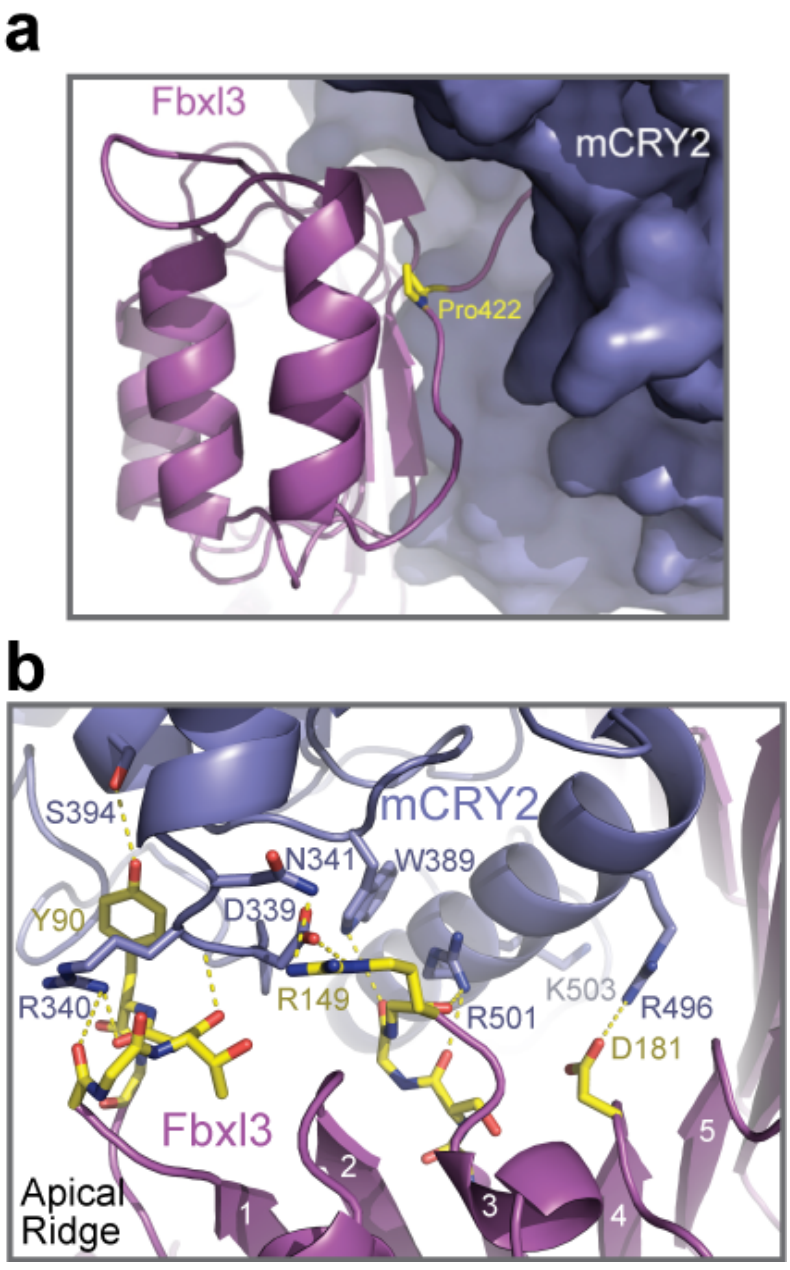

Supplementary Figure 8. Sequence alignment of select regions of vertebrate cryptochromes. Sequence alignment of the interface loop (a), the phosphate loop (b), and the protrusion motif (b) in vertebrate cryptochromes from *Mus musculus* (Mm), *Homo sapiens* (Hs), *Xenopus laevis* (Xl), *Gallus gallus* (Gg), and *Danio rerio* (Dr). Two previously documented phosphorylation sites are boxed. Strictly conserved residues are in red.

a.

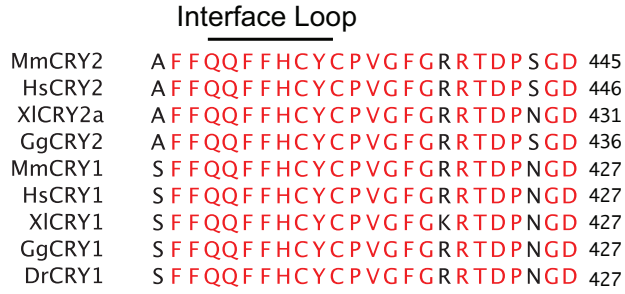

b.

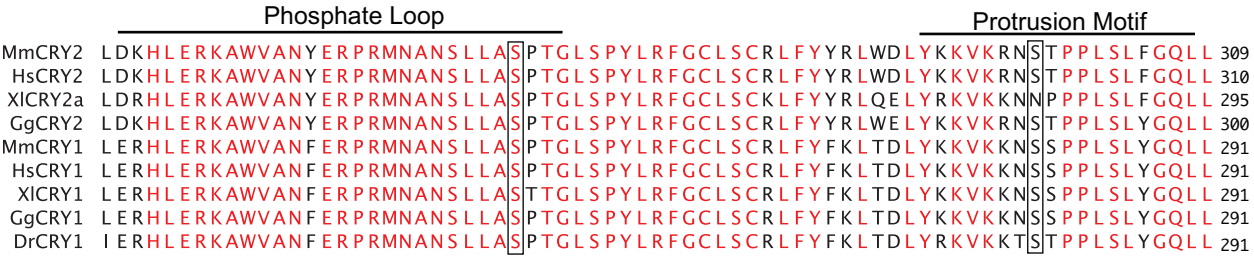

Supplementary Figure 9. Interface between mCRY2 and Fbxl3-LRR-C. Top: A cut-away view of the interface between mCRY2 (blue) and the Fbxl3 LRR-C subdomain (magenta). For clarity, LRR11, LRR12, and the C-terminal tail of Fbxl3 are not shown. Select residues chosen for mutational studies are shown in sticks. Fbxl3 E336 accepts two hydrogen bonds (orange dash lines) from backbone NH groups of the mCRY2 CSS region. While packing against several hydrophobic residues, the hydroxyl group of Fbxl3 Y292 forms a hydrogen bond with mCRY2 K503. Bottom: Locations of important interface amino acids identified by mutational analysis.

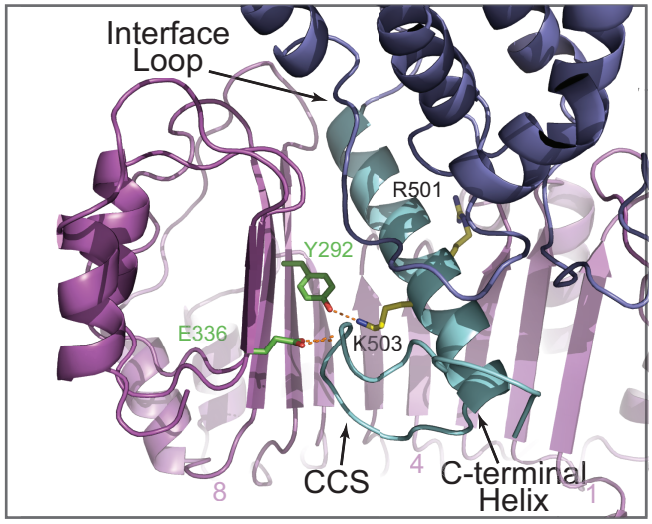

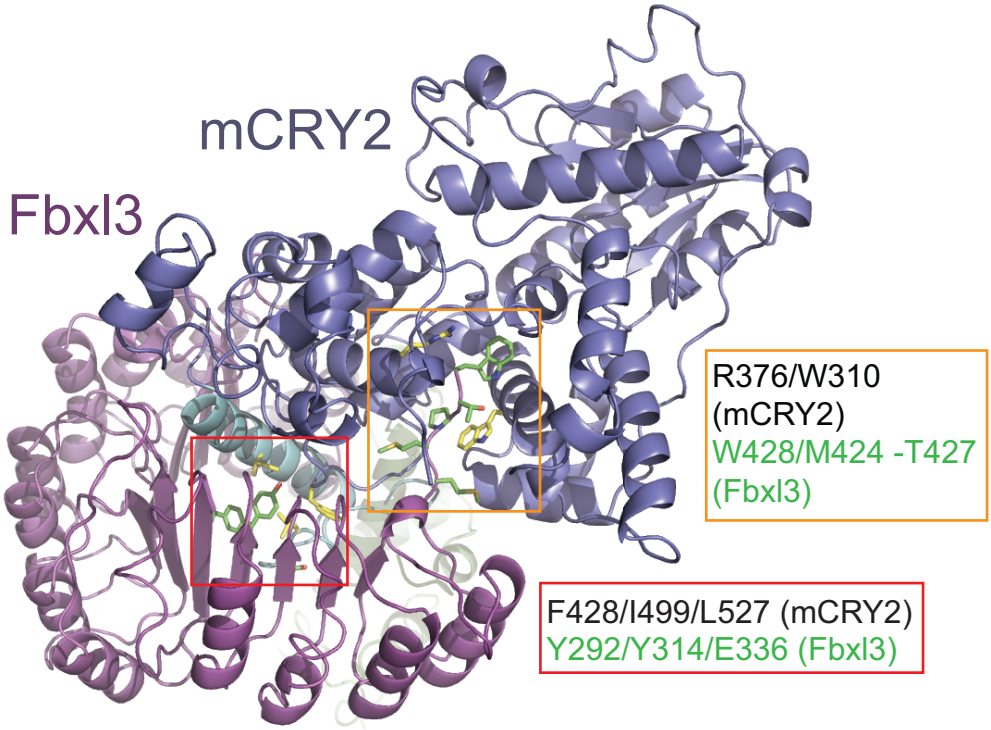

Supplementary Figure 10. Period competes with Fbxl3 for binding CRYs. **a,** PER2-bound mCRY2 is completely devoid of Fbxl3. HEK293T cells were transfected with cDNAs encoding Myc-mPER2 and increasing amounts of a plasmid encoding Flag-mCRY2. Myc-mPER2 was immunoprecipitated from whole cell lysate (WCL) with anti-Myc resin. Immunoblotting was performed for the indicated proteins. **b,** The abundance of PER2 had a direct effect on the stability of both CRY1 and CRY2. Accumulation of CRY1 and CRY2 in the presence of increasing amounts of PER2. L, H, and EV stand for low, high exposure and empty vector.

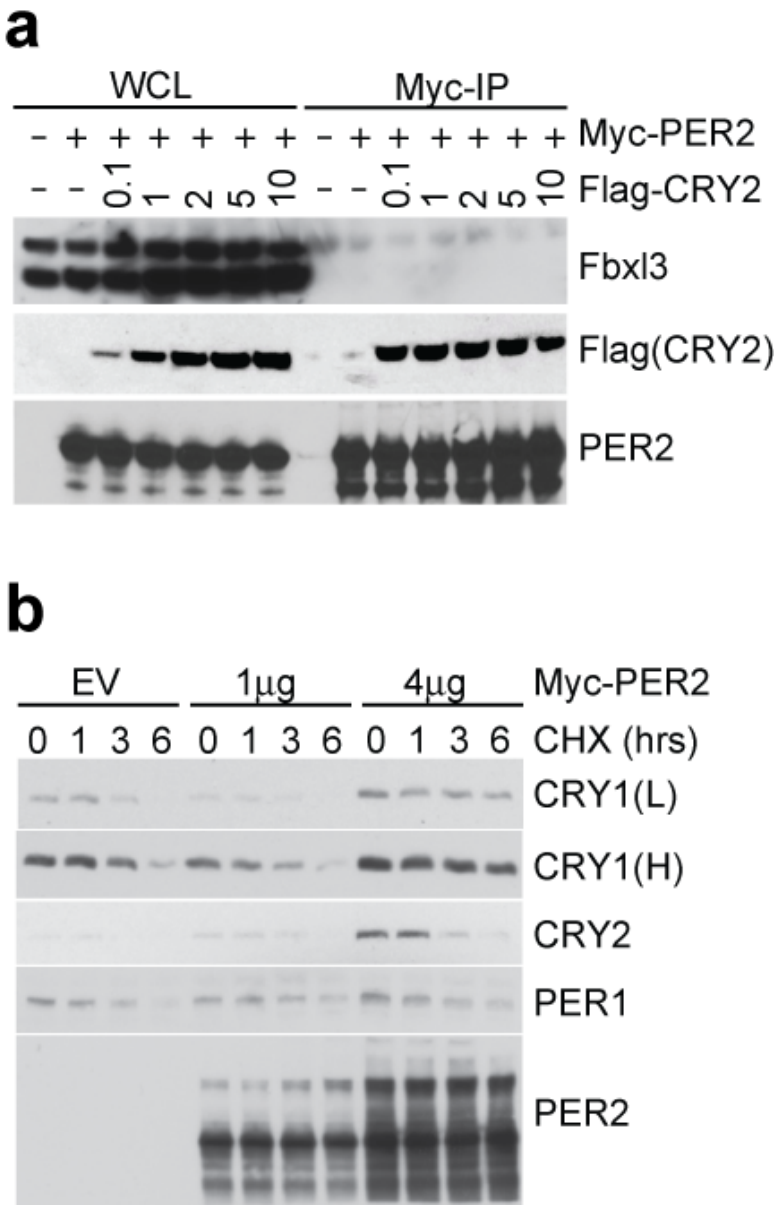

Supplementary Figure 11. Phosphorylation sites mapped onto the mCRY2 structure. The mCRY2-Fbxl3-Skp1 structure is shown in cartoon representation. Three previously documented phosphorylation sites for CRY2 (red) and CRY1 (grey, in parentheses) are indicated. Three PER-binding residues of mCRY2 are labeled, together with the Fbxl3 C-terminal Trp428 residue. Two key structural motifs, the phosphate loop and the protrusion motif are indicated.

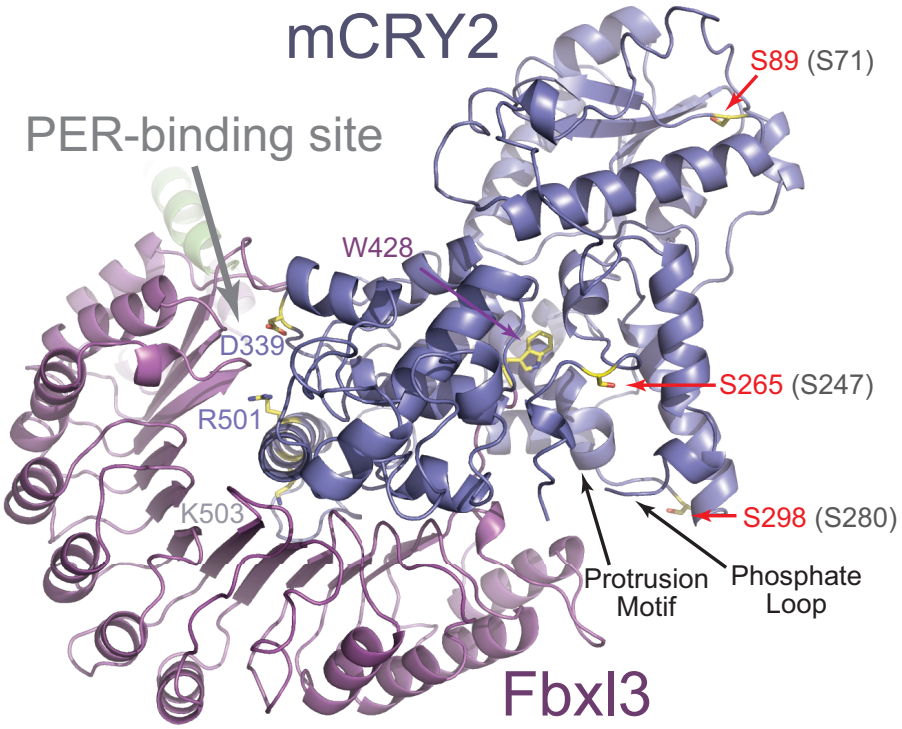

Supplementary Figure 12. Comparison of LRR-containing F-box proteins with known structures. Different Fbxl proteins with a variable number of LRRs pack against the Skp1-F-box structural module from a similar angle as seen in the ribbon diagrams of the Skp1-Fbxl3 (human), Skp1-Skp2 (human, ref. 40), and Skp1-TIR1 (plant, ref. 41) complexes (top row). The Skp1-F-box modules in these complexes are presented in the same orientation as indicated by a reference point labeled with a red arrow. All substrates are docked to the concave side of the LRRs as seen in the ribbon diagrams of the full Skp1-Fbxl-substrate complexes (middle row) and are presented toward the Rbx1 subunit of SCF, which recruits the ubiquitin-charged E2 (bottom).

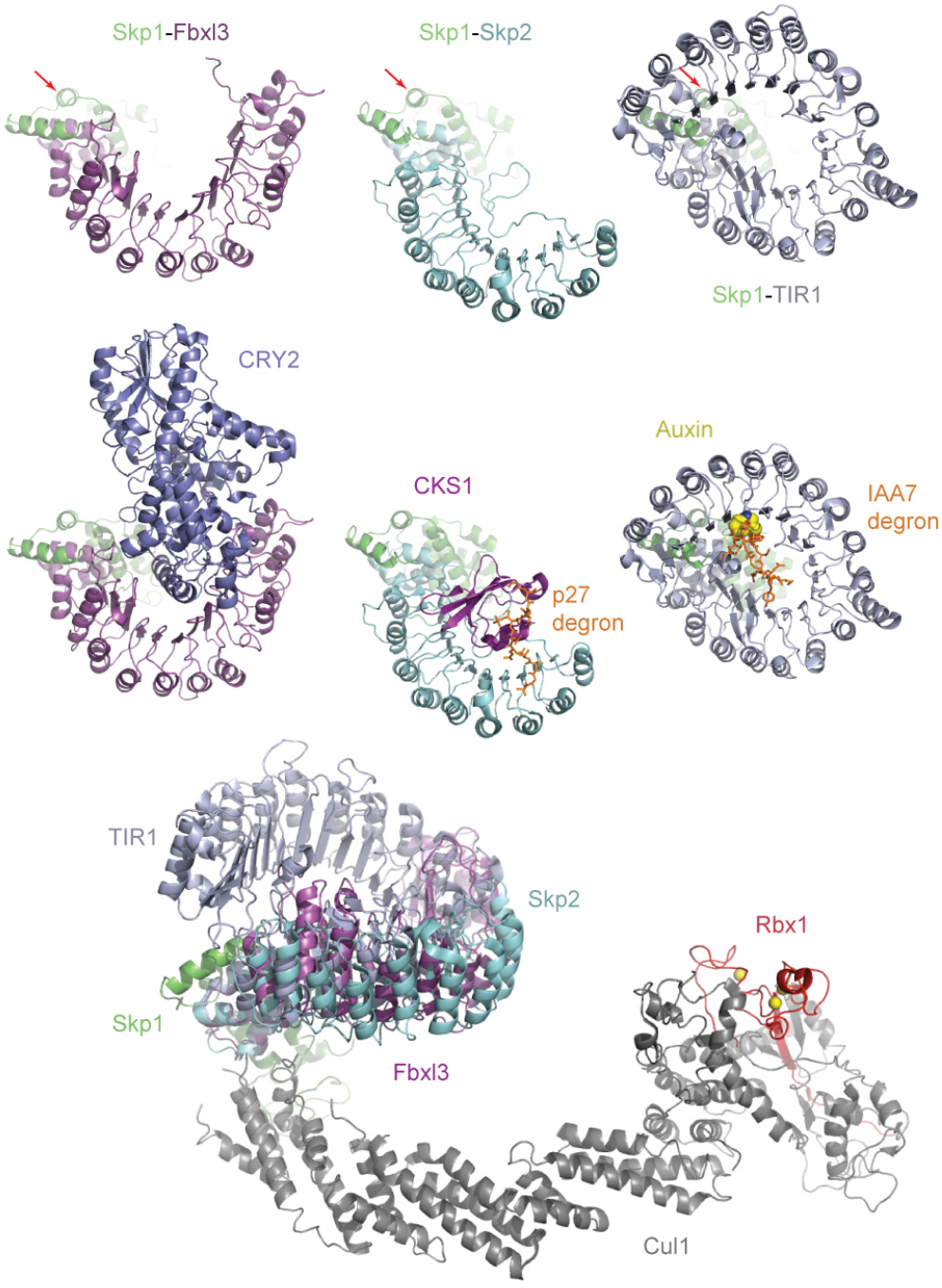

Supplementary Methods

Native mass spectrometry analysis

Prior to analysis, mCRY2 solutions were exchanged into aqueous 1.00 M ammonium acetate using gel filtration chromatography. The fractions containing mCRY2 were then concentrated using a MicroSep centrifugal device (Pall Life Sciences, Ann Arbor, MI) with a 10 kDa molecular weight cutoff. The concentrated solutions were then diluted using 1 M ammonium acetate buffer and re-concentrated three additional times. The mCRY2-Fbxl3-Skp1 sample was buffer exchanged into an aqueous 300 mM ammonium acetate solution at pH 8 using a Spin-X UF 500 μL Centrifugal Concentrator with a 10 kDa molecular weight cutoff (Corning, Inc., Corning, NY). All experiments were performed using nanoelectrospray ionization and a Waters Synapt G2 HDMS mass spectrometer. All spectra were calibrated externally using a solution of cesium iodide (16 mg/ml in 50/50, water/isopropanol).

Supplementary Table 1. Data collection, phasing and refinement statistics.

	mCRY2-Fbxl3-Skp1		mCRY2-PHR	mCRY2-PHR-FAD
	Native	$KAu(CN)_2$		
Data collection				
Space group	$P3_121$	$P3_121$	$P4_3$	$P4_3$
Cell dimensions				
a, *b*, *c* (Å)	125.4 125.4 145.7	125.6 125.6 146.0	68.9 68.9 127.5	97.5 97.5 128.8
α, β, γ (°)	90 90 120	90 90 120	90 90 90	90 90 90
Resolution (Å)	2.7	3.0	2.7	2.2
R_{sym} or R_{merge}	0.094	0.092	0.066	0.058
$I/\sigma I$	27.9 (4.4)	30.4 (2.5)	45.0 (7.6)	37.2 (2.5)
Completeness (%)	100 (100)	89.1 (91.4)	99.9 (100)	99.9(98.9)
Redundancy	5.5 (5.6)	7.8 (7.7)	5.1 (5.2)	6.2 (5.3)
Refinement				
Resolution (Å)	47.5-2.7		48.7-2.7	43.6-2.2
No. reflections	36840		16379	60952
R_{work}/ R_{free}	21.0/27.6		24.4/28.7	19.7/23.8
No. atoms	8432		3822	8109
Protein	8279		3821	7740
Ligand/ion				106
Water	153		1	263
B-factors				
Protein	53.2		111.1	70.1
Ligand/ion				
Water	40.7		60.4	53.5
R.m.s deviations				
Bond lengths (Å)	0.009		0.009	0.009
Bond angles (°)	1.4		1.3	1.2

Supplementary Table 2. Comparisons of mCRY2-PHR and select cryptochromes and (6-4)-photolyases of known structures.

	PDB	Identity (%)	Similarity (%)	RMSD (Å)	Equivalent Cα
Dm(6-4)-photolyase	3CVU	53	69	1.1	431
At(6-4)-photolyase	3FY4	50	67	1.2	425
*Dm*CRY *	3TVS	41	57	1.4	416
*At*CRY1	1U3C	28	45	1.6	381

Dm: Drosophila malanogaster
At: Arabidopsis thaliana
* Type I animal cryptochrome

Supplementary Discussion

Binding of reduced FAD to mCRY2-PHR

The mCRY2-PHR crystals were soaked with 1 mM FAD in the presence of dithionite, which is a known FAD reducing agent. After structure determination by molecular replacement, weak electron density was detected at the FAD-binding pocket, suggesting that reduced FAD does not bind mCRY2-PHR with the same affinity as its oxidized form. Because FAD did not affect the C-terminal degradation of mCRY2 (1-544) and mCRY2 (1-527) in the presence or absence of dithionite, we concluded that the CCS region does not alter the binding of reduced or oxidized FAD in the isolated form of mCRY2. However, it remains highly possible that certain CRY-binding proteins might modulate interactions between CRYs and FAD in either reduced or oxidized form.

The role of two cysteine residues and a nearby salt bridge at the mCRY2-Fblx3 interface

Near the apical ridge of Fbxl3-LRR-C, Fbxl3-C340 and mCRY2-C430 are close to each other within the disulfide bond distance (Figure 6b, c). Although intracellular disulfide bond formation is unusual, this raised the possibility that the two residues might play a role in mediating Fbxl3-mCRY2 interaction. We mutated each of the two residues and tested their effects on mCRY2 binding to Fbxl3. As shown in Figure 6d and 6e, neither point mutation had any detectable impact to the association of the two proteins, suggesting that the two cysteine residues are not critical for complex formation. Similarly, point mutation of the nearby Fbxl3-E368 residue (Figure 6b), which forms a potential inter-molecular salt bridge with mCRY2-R439 located at the helix C-terminal to the interface loop, showed no effect to complex formation (Figure 6d).

Intracellular concentration of free FAD

Oxidized FAD binds unmodified and isolated mCRY2 with a modest affinity, which appears to be above the concentration of free FAD in the cell. Most known cellular flavoproteins bind FAD as a prosthetic group with an extremely high affinity. Despite decades of FAD research, the concentration of free FAD in the mammalian cells has not been reported to our knowledge. Although it is generally believed that free FAD concentration is "extremely low" or "zero", Tu & Weissman have reported that wild type yeast cells contain ~3 μM free FAD, which is critical for the optimal activity of the ER-resident protein Ero1p that mediates oxidative protein folding. Using HeLa cell lysate filtrated through a membrane with a molecular weight cut-off of 10 kDa, we estimated that the free FAD concentration is around 0.1 μM. The levels of free FAD in different cells remain to be systematically determined and are expected to vary. For instance, the total FAD concentration during adipogenic differentiation of 3T3-L1 cells has been reported to increase by more than 15 fold. This change markedly affects the activity of the lysince-specific demethylase-1 enzyme (LSD1), whose function is dependent on FAD (Hino S. et al. 2012 Nature Commun. 3:758).

References

B.P. Tu & J.S. Weissman 2002 Mol. Cell 10:983-994.
Hino S. et al. 2012 Nature Comm. 3:758.